POLITECNICO DI TORINO

Master Degree course in Automotive Engineering

Master Degree Thesis

Equivalent consumption minimization strategy for a fuel cell catamaran

Supervisors
Prof. Federico Miretti
Prof. Daniela Anna Misul

Candidate
Stefano Michela

Academic Year 2024-2025

Abstract

The Monaco Energy Boat Challenge (MEBC) is an international competition promoting innovation in sustainable marine propulsion. In the endurance race, one of its main events, teams aim to complete as many laps as possible under a strict energy budget.

This work presents a control strategy based on the Equivalent Consumption Minimization Strategy (ECMS) for a hybrid catamaran powered by a lithium-ion battery and a PEM fuel cell.

A quasi-static powertrain model is used to simulate the system's behavior and calibrate optimal equivalence factor (λ) values via a bisection algorithm, accounting for varying speed profiles and hydrodynamic drag conditions. This calibration process results in a lookup table-based controller, enabling real-time implementation of ECMS. The strategy is developed in MATLAB and validated through dynamic simulations in Simulink, which replicate the full hybrid architecture, including both electrical and mechanical subsystems.

Contents

Chapter 1

Introduction

1.1 Team

PoliTo H2Fly is a team founded in September 2023 with the goal of studying powertrain solutions for the marine sector. The research activity is carried out through the design and construction of a racing boat to compete in the Monaco Energy Boat Challenge. This thesis focuses on a study dedicated to the team's second prototype, NEUS, launched in its first version in July 2025.

Figure 1.1. Team photograph from the 2025 season.

1.2 Competition

The Monaco Energy Boat Challenge, organized by the Yacht Club de Monaco, is an international competition that promotes innovation in sustainable marine propulsion. In Fig.1.2 a photo of the team participating in the 2025 edition. The event encourages the use of alternative energy

sources such as electricity, hydrogen, and solar power. Participants compete in three distinct classes, Open Sea, Solar, and Energy, each governed by specific rules.

Figure 1.2. Monaco Energy Boat Challenge edition 2025.

This work focuses on an Energy Class prototype, which allows hybrid systems powered by carbon-free energy sources like hydrogen fuel cells and batteries. To ensure fairness, a total energy cap of 10 kWh is imposed, adjusted by an energy factor that accounts for source efficiency (0.4 for hydrogen, 1 for batteries). The challenge provides a standardized catamaran hull to all teams, focusing the study on structural design and powertrain.

The technical rules, taken from the official *Monaco Energy Class Technical Rules 2025 V5* [1], that need to be reported in the study for completeness are listed below:

- ENERGY REQ 7 v1.1: At any moment, the maximum energy stored by a boat shall remain under 10kWh according to the following calculation. The total energy stored is define by: $E_{tot} = \sum E_i \times f_i$
  With:
  - E_i the energy stored by the source
  - f_i the energy factor defined by the following table

Energy source (E_i)	**Energy factor** (f_i)
Hydrogen	0.4
Battery	1.0
Flywheel	0.5
Heat	0.3
Compressed air	0.2

- ENERGY REQ 48 v3.0: The overall weight excluding the hulls shall not exceed 250kg. *Note: The boat will be weighted with the hulls and the pilot. The hulls are supposed to be 65 kg.*

Races in the Energy Class include:

- Slalom: Speed race on a defined course to test maneuverability.

- Sprint: One kilometer straight-line trial to be completed in the shortest possible time.
- Championship: A series of head-to-head regattas.
- Endurance: A four-hour circular circuit race where the goal is to complete the maximum number of laps. In Fig.1.3 the endurance track.

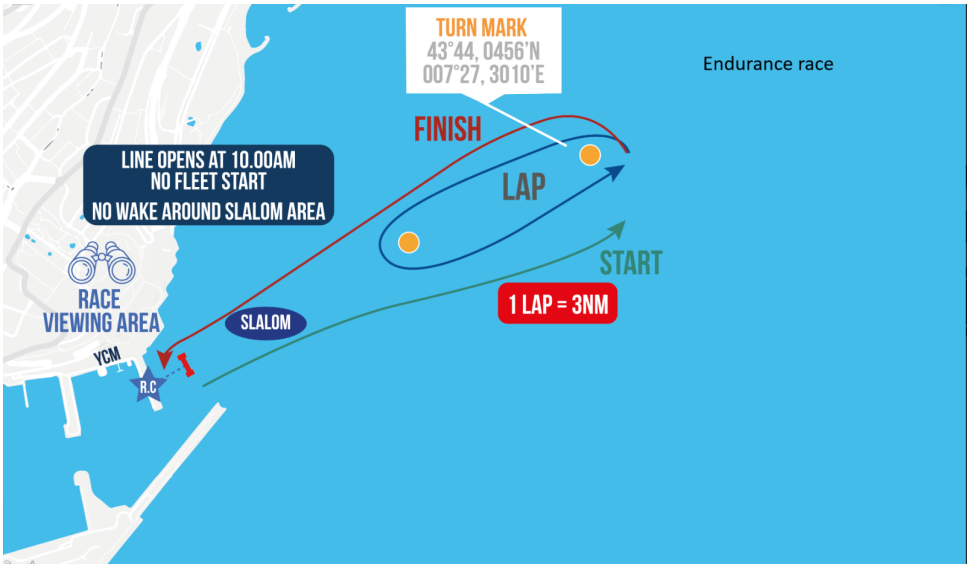

Figure 1.3. Endurance race track.

The endurance race is particularly significant as it awards double points compared to the one-lap race, making it the primary focus in both boat design and simulation.

1.3 Motivation and workflow

The team 's prototype features a hybrid powertrain architecture that combines a 7kWh battery pack with a 13L 200bar hydrogen tank supplying a 2kW fuel cell. The integration of hydrogen into the system is driven by the team's commitment to deepening its study and optimizing its integration and efficiency, ideally overcome the nominal efficiency of 40%. In fact, within the competition framework, the energy stored as hydrogen is weighted at 0.4kWh per each onboard kWh. Therefore, any efficiency improvement beyond this factor provides a significant boost to the boat 's effective energy capacity. In this context, the role of the Energy Management System (EMS) is critical. It must not only enable the systems overall functionality but also optimize its performance, while being capable of managing all possible operating conditions, ranging from high-range to high-power demands. Among the various races, the endurance race presents the greatest opportunity for optimization, and thus the analysis in this work is centered on it. In contrast, the other events, slalom, sprint, and championship, can typically be covered using the battery alone, while situations requiring higher motor power can be addressed by operating both the battery and the fuel cell simultaneously at full power.

Within this context, the optimization of the hybrid system developed by the team plays a crucial role. A key objective is to implement a strategy that efficiently distributes the power demand between the battery and the fuel cell. Given the significant differences in their power delivery capabilities, achieving effective synergy between the two sources is essential to meet the propulsion requirements. This thesis constitutes a first study on the topic, with particular focus

on enhancing the system efficiency over long distances, a condition typical of the endurance race, one of the main challenges the prototype must tackle during the competition.

To address this, the project follows a two-phase workflow: first, a quasi-static modeling phase is used to define optimal equivalent factor (eqFactor) values for controller design; second, the resulting controller is validated through dynamic simulations using a comprehensive Simscape model of the full powertrain. The objective is to achieve a balanced and efficient power distribution strategy between the battery and fuel cell, with the ultimate aim of enhancing energy utilization over long-range missions.

1.4 Boat

This work was carried out using the 2025 project for the Energy Class, a hybrid fuel cell and battery-powered catamaran, with the regulatory limits set as parameters.

Figure 1.4. Boat during the race in the 12th Monaco Energy Boat Challenge.

All the specifications of the prototype, as used for the analyses:

The battery pack is composed of 16S 1P. In Table 1.1, the parameters of a single cell are reported.

Nominal Voltage (V)	3.2
Nominal Capacity (Ah)	134
Max Discharge Current (A)	268
Internal Resistance (Ω)	0.00025
Total Capacity (Wh)	431.48
Max Power (W)	857.6
Max Charge Voltage (V)	3.65

Table 1.1. Battery cell parameters - SVOLT LI-134F 3.2V 134Ah.

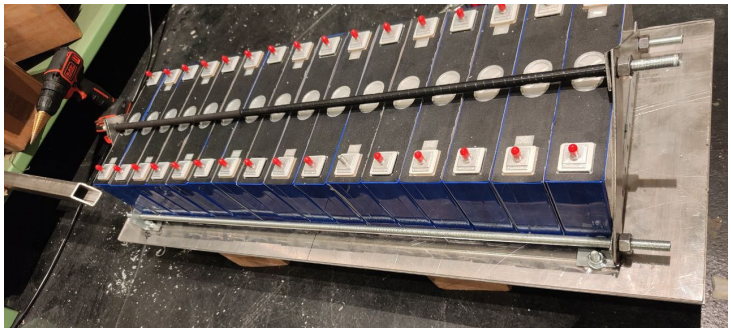

Figure 1.5. Assembling of the battery pack on the dedicated plate.

The fuel cell used is an PEM Horizon H2000, open-cathode typology. The model of the fuel cell used for the simulation is simplified as explained in [2]. The open-circuit voltage and internal resistance values are the results of this simplification and are used to characterize the cell.

Number of Cells	48
Maximum Power (W)	2000
Maximum Current (A)	70
Open-Circuit Voltage (V_{oc})	41.56
Internal Resistance (Ω)	0.1473

Table 1.2. Fuel cell parameters - H2000.

The propulsion system, Fig.1.6, consists of a 48V, 10.5 kW BLDC electric motor operated with a stock motor controller, whose parameters are reported in Table 1.3.

Figure 1.6. Propulsion system, 48V 10.5 kW

Max power (P_{max})	10500	[m]
Max current (I_{max})	220	[A]
Max torque (T_{max})	36.96	[Nm]
Base speed (n_{base})	2120.7	[rpm]
Max speed (n_{base})	2400	[rpm]
Motor efficiency (η_m)	0.93	
Driver efficiency (η_{drive})	0.95	

Table 1.3. Electric motor parameters.

The competition allows for the replacement of the propeller between races. For this reason, the hydrodynamics division developed two different propellers. In the analysis presented here, the propeller selected is the one optimized for the endurance race. Its parameters are listed in Table 1.4.

Diameter (D)	0.34 [m]
Trust coefficient (K_T)	0.25
Torque coefficient (K_Q)	0.05

Table 1.4. Endurance propeller parameters.

Figure 1.7. 3D printed propeller with optimized design for the endurance race.

Chapter 2

Energy Management Strategies

In HEVs the traction power demand can be provided in several different ways. Especially in a fuel cell hybrid system two porpoise must be taking in account. On one side the higher performance in terms of efficiency have to be reached, defining the optimal split between battery power and fuel cell power, and consequently the hydrogen consumption. Moreover in this type of system the battery has higher power capability and lower response time, so is in charge to them cover the peak and the situation where the fuel cell is not fast enough to provide the required power [2]. Specifically in this powertrain the fuel cell is only able to provide 2 kW of power in nominal condition, while the eMotor can reach up to 10.5 kW of absorbed power. The battery is than able to provide at least the remaining necessity, with 268 A continuous current.

2.1 The Energy Management System

The EMS architecture presented in this study is schematically illustrated in Fig.2.1. The drag condition recognizer identifies the most suitable drag curve based on the motor power demand and the actual boat speed. Once the drag condition is selected and the speed is known, the EMS determines the optimal power split between the battery and the fuel cell. Specifically, it provides the appropriate fuel cell current setpoint, which is regulated through a dedicated DCDC converter.

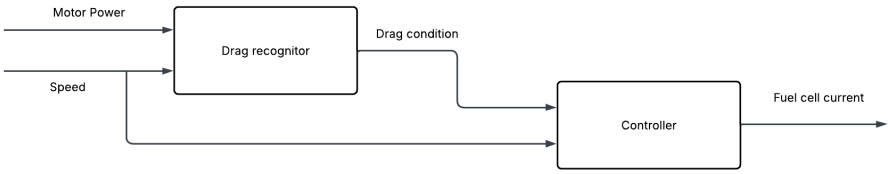

Figure 2.1. EMS high level block diagram.

2.2 Energy Management Strategies review

Different energy management strategies can be categorized, as proposed in [2], primarily based on the knowledge of future driving conditions and the type of control theory applied. Regarding the first classification, non-causal strategies can only be employed when the mission profile is well known, such as in public transport applications or, as in this case, within a defined race envelope. Causal strategies must be used in all other cases where the driving cycle is unpredictable, which represents the majority of real-world scenarios. The second classification

distinguishes between heuristic energy management strategies, which are based on intuitive rules and empirical correlations, and optimal energy management strategies, which involve formulating a control problem and mathematically defining a performance index to be minimized. Concerning the study presented, the next sections will further explore the classification based on control theory, established that the particular case under consideration assumes a known mission profile defined by the race strategy.

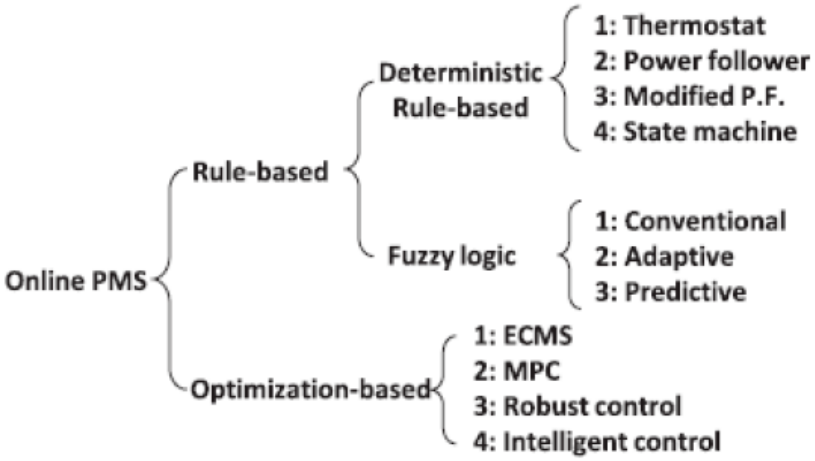

Figure 2.2. Energy management strategies review [3].

2.2.1 Heuristic energy management strategies

In a heuristic or rule-based strategy, the Energy Management System (EMS) operates based on intuitive rules derived from various vehicle behaviors. Each manufacturer can tune the EMS according to specific requirements, which makes it difficult to define a general optimization law. As a result, the EMS is individually calibrated for each product, taking into account constraints related to efficiency, performance, and component health, particularly for the battery pack. A common approach involves mapping the strategy on a State of Charge (SOC) vs. driver torque request diagram to determine the appropriate power split. An example of such a rule-based mapped strategy is shown in Fig. 2.3, extrapolated from [2]. For further examples and a more in-depth discussion on heuristic methods, refer to [2].

2.2.2 Optimal energy management strategies

Optimal strategies are based on control theory, requiring the definition of a performance index, typically denoted as J, which is then minimized. The optimization problem can take various forms depending on the selection of the performance index J, the state variables $x(t)$, and the imposed constraints. A common choice for the performance index is the total fuel consumed over the mission duration, represented as in Eq.2.1.

$$J = \int_0^{t_f} \dot{m}_f(w(t), u(t))\, dt \tag{2.1}$$

where $\dot{m}_f$ is the fuel consumption rate, and $w(t), u(t)$ are the state and control variables, respectively.

Several optimal control strategies exist, each with distinct trade-offs between computational complexity and performance [7] [8]:

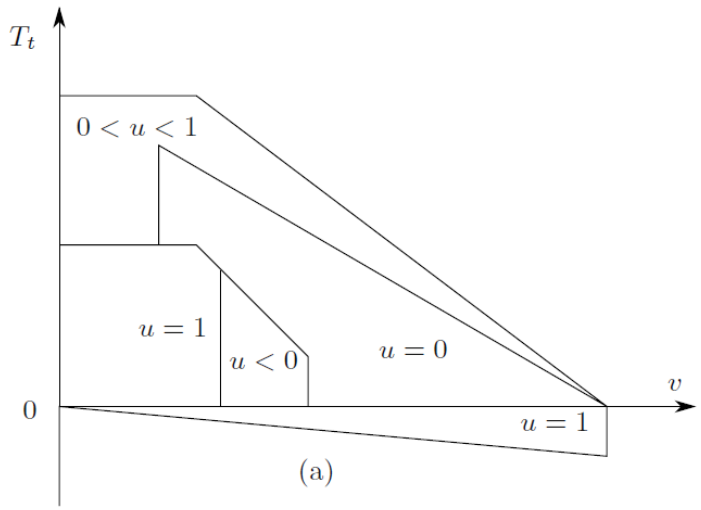

Figure 2.3. Example of heuristic energy-management strategy for a parallel HEV. SOC (u) vs Required torque (T_t) [2].

- Dynamic Programming (DP): Provides high-accuracy solutions and is often used as a benchmark, but is computationally expensive and unsuitable for real-time control.
- Pontryagin's Minimum Principle (PMP): Offers results close to the global optimum with lower computational cost, although its performance is sensitive to the initialization of costate variables.
- Extremum Seeking (ES): Capable of real-vehicle application and near-optimal fuel consumption results, though less effective at accounting for fuel cell degradation.
- Equivalent Consumption Minimization Strategy (ECMS): Achieves good real-time performance and balanced trade-offs between fuel economy and fuel cell lifetime, but relies on functional analysis, which can be difficult to interpret.
- Neural Networks (NN): Provide high real-time quality and near-optimal results once trained, but require large datasets and significant training effort.

2.3 Equivalent Consumption Minimization Strategy

Non-causal control methods, also referred to as offline or global optimization techniques, are based on the assumption that the entire driving profile or mission cycle is known in advance. These methods are widely used for benchmarking purposes and for deriving optimal energy management strategies in hybrid and fuel cell vehicles. Their primary objective is to compute the optimal power split among the available energy sources (e.g., battery and fuel cell) that minimizes a given cost function, typically fuel or hydrogen consumption, over the entire driving cycle.

These approaches can be classified into two main categories: static optimization and dynamic optimization

- Static optimization techniques assume that the system is in a steady-state and optimize over average or root mean square values of the power demand. While computationally efficient, these methods can only be applied under restrictive conditions, such as periodic or quasi-steady operation, and often fail to capture the transient behavior of real-world driving cycles.

- Dynamic optimization techniques, including Dynamic Programming (DP) and Pontryagin's Minimum Principle (PMP), take into account the system dynamics and constraints over time. These methods are more suitable for complex energy systems with dynamic behaviors, such as fuel cell hybrid electric vehicles.

Among these, Dynamic Programming is a widely used method due to its ability to guarantee a globally optimal solution by recursively solving the optimal control problem over a discretized time-state space. The main limitation of DP lies in its high computational burden, which grows exponentially with the number of states and control variables, a phenomenon known as the 'curse of dimensionality'. Nonetheless, it serves as a gold standard for evaluating the performance of real-time strategies and verifying theoretical results.

Pontryagin's Minimum Principle (PMP) offers an alternative formulation for dynamic optimization by providing necessary conditions for optimality. Unlike DP, PMP does not require discretizations of the state and time spaces, which makes it more efficient in terms of memory usage. However, solving the resulting two-point boundary value problem is often challenging, especially in systems with non-linear dynamics or non-convex cost functions.

2.3.1 Pontryagin's Minimum Principle

The Pontryagin's Minimum Principle (PMP) provides a theoretical foundation for deriving optimal control laws by minimizing a cost function (e.g., fuel consumption or hydrogen usage) over a driving cycle, while accounting for dynamic constraints such as battery state of charge (SOC). Under certain assumptions, especially in quasi-static conditions, the optimal control can be determined by minimizing an equivalent instantaneous cost, which leads to the practical implementation known as the Equivalent Consumption Minimization Strategy (ECMS).

In most practical cases, the relationship between the initial value of the costate variable λ and the final value of the state trajectory (e.g., battery SOC, $\xi(t_f)$) is monotonic. This means that only one unique value of λ satisfies a terminal constraint, such as ending the driving cycle at a target SOC ξ_t. Due to this monotonic relationship, numerical methods such as the bisection algorithm can be used to iteratively adjust λ until the terminal condition is met.

ECMS approximates PMP in real time by assuming a constant or slowly-varying λ, transforming the optimal control problem into an instantaneous minimization of equivalent fuel consumption. This balance between optimality and computational efficiency makes ECMS a widely adopted strategy in real-time energy management for hybrid and fuel-cell vehicles [2].

The total cost to be minimized must be defined as follow and is called performance index:

$$J = \int_{t_0}^{t_f} v(x(t), u(t), t)dt \tag{2.2}$$

In the previous equation the derivative of the state x is function of the state, other than input and time.

$$\dot{x}(t) = f(x(t), u(t), t) \tag{2.3}$$

To define and solve the optimization problem firstly is required to evaluate the Hamiltonian equation of the dynamic system (Eq.2.4) the state equation (Eq.2.5), costate equation (Eq.2.6)and control equation (Eq: 2.7).

$$H(x, p) = v(x(t), u(t), t) + p \cdot f(x(t), u(t), t) \tag{2.4}$$

$$\dot{x}(t) = \frac{dH}{d\lambda} \tag{2.5}$$

$$\dot{\lambda}(t) = -\frac{dH}{dx} \tag{2.6}$$

Following the costate equation as defined in 2.6 the costate value can be a constant only if the Hamiltonian function is not a function of the state. If not the costate λ will be a trajectory. [4].

The minimization must be carried out in such a way that

$$\frac{dH}{du} = 0 \tag{2.7}$$

Considering as a necessary condition for u to minimize the performance index:

$$\dot{\lambda}(t) = -\frac{dH}{dx} \tag{2.8}$$

and

$$H(x^*, u^*, p^*) = min_{u \in U} H(x, u, p) \tag{2.9}$$

2.3.2 Control law definition

In this section, the optimal control problem is formulated with the objective of minimizing total hydrogen consumption. The performance index to be minimized corresponds to the total fuel consumption over the entire driving cycle:

$$J = \int_{t_0}^{t_f} P_f(t) dt \tag{2.10}$$

The control problem is defined below

input	P_b
state	σ (SOC)
cost	$\dot{m}_{H_2}$

Table 2.1. Control problem definition

State dynamic:

$$\dot{\sigma} = -\frac{1}{3600 C_b} \frac{V_{batt,oc} - \sqrt{V_{batt,oc}^2 - 4 R_{batt} P_{batt}}}{2 R_{batt}} \tag{2.11}$$

Cost function:

$$cost = \dot{m}_{H_2}(P_b, P_d) = \frac{M_{H_2} N_{fc}}{2F} \cdot i_{fc} \tag{2.12}$$

$$i_{fc} = \frac{V_{fc,oc} - \sqrt{V_{fc,oc}^2 - 4 R_{fc} P_{fc}}}{2 R_{fc}} \tag{2.13}$$

Where i_{fc} is obtained by a simplified model of the fuel cell, linearizing the polarization curve of the fuel cell.

At this point the Hamiltonian function of the system can be defined as explained before.

$$H = \dot{m}_{H_2} + \lambda \dot{\sigma} \tag{2.14}$$

Costate equation:

$$\dot{p} = -\frac{dH}{d\sigma} = -\frac{d}{d\sigma}(m_{H_2} + \lambda \frac{i_b}{C_b}) = -\frac{di_b}{d\sigma} \tag{2.15}$$

If we make the assumption of V_{oc} and R of the battery constant we can consider the costate as a constant due the fact that H is not dependent of the state.

The following derivation aims to minimize the previously defined cost function, enabling its use, once the costate value is known, to determine the optimal power split between the fuel cell and the battery.

The two derivatives are respectively:

$$\frac{\partial \dot{m}_{H_2}}{\partial P_{fc}} = \frac{M_{H_2} N_{fc}}{2F} \frac{1}{\sqrt{V_{fc,oc}^2 - 4R_{fc}P_{fc}}} \tag{2.16}$$

$$\frac{\partial \dot{\sigma}}{\partial P_{fc}} = \frac{1}{3600 C_b} \frac{1}{\sqrt{V_{batt,oc}^2 - 4R_b(P_d - P_{fc})}} \tag{2.17}$$

Than the problem law is defined as below

$$0 = \frac{M_{H_2} N_{fc}}{2F} \frac{1}{\sqrt{V_{fc,oc}^2 - 4R_{fc}P_{fc}}} + s \cdot \frac{1}{3600 C_b} \frac{1}{\sqrt{V_{batt,oc}^2 - 4R_b(P_d - P_{fc})}} \tag{2.18}$$

Solved in Pfc, as is used to evaluate the power split:

$$P_{fc} = \frac{-3240000\, C_b^2 M^2 N^2 V_b^2 + 12960000\, P_d R_b C_b^2 M^2 N^2 + F^2 V_{fc}^2 s^2}{4\left(3240000\, R_b C_b^2 M^2 N^2 + R_{fc} F^2 s^2\right)} \tag{2.19}$$

than

$$P_{fc} = \frac{-3240000 \mu 1 V_b^2 + 12960000 P_d R_b \mu 1 + F^2 V_{fc}^2 s^2}{4(3240000 R_b \mu 1 + R_{fc} F^2 s^2)} \tag{2.20}$$

with

$$\mu 1 = C_b^2 M^2 N^2 \tag{2.21}$$

Chapter 3

Design and implementation of the controller

3.1 Hydrodynamic drag analysis

Evaluating drag in the marine sector is a complex task due to the large number of variables involved. Given this complexity, and considering the relative low importance of drag in this study's focus on energy management strategies, an unconventional approach has been adopted.

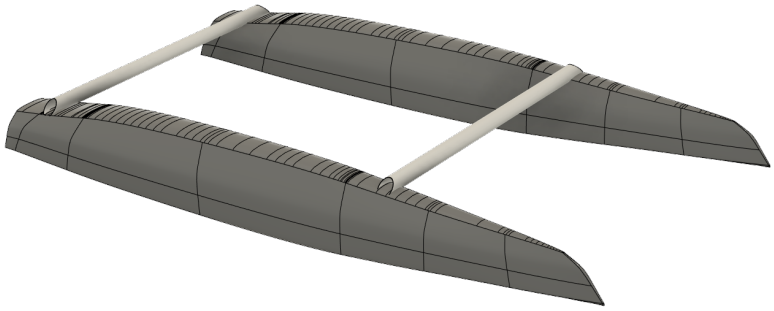

Figure 3.1. Hull provided by the competition for the energy class.

The competition directly provides drag curves for the racing hulls (Fig.3.1); however, these are based on perfectly calm water conditions, which are not entirely representative of real-world operation. Nonetheless, this first curve can be considered the best-case scenario. The worst-case drag curve was instead derived from empirical data collected during the 2024 competition, an event characterized by particularly rough sea conditions, nearly leading to race suspension. In between these two defined drag curves, two additional drag curves were extracted, resulting in a total of four drag scenarios considered for the controller design.

The four drag curves are shown in Fig.3.2.

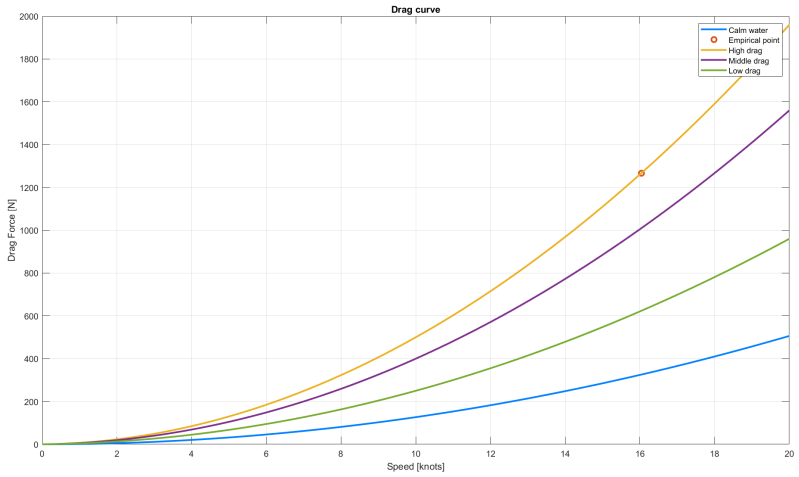

Figure 3.2. Four drag curves used for the controller design.

3.2 ECMS implementation in design phase

The algorithm discretizes the battery power into 100 equally spaced values. For each of these discrete battery power levels, the hybrid powertrain model simulates the corresponding system response, including fuel cell power output, hydrogen consumption, and feasibility checks based on system constraints. The equivalent fuel consumption is then computed according to Eq.3.1.

$$equivalentConsumption = \dot{m}_{\mathrm{H_2}} + \lambda \cdot (SOC_i - SOC_{i+1}) \tag{3.1}$$

where λ is the equivalence factor and i is the time instant.

The minimum feasible value of the equivalent consumption is selected, and the corresponding battery power value is identified as the optimal battery power.

3.3 Quasi-static model

To design the controller using an offline optimization approach, a quasi-static model of the entire powertrain was developed. This model includes two states: the State of Charge (SOC) of the battery and the State of Tank (SOT) representing the hydrogen storage level. However, the SOT is used solely to monitor the remaining hydrogen in the tank and does not play a role in the control strategy.

3.3.1 Battery

The battery model implemented in this study is based on a simplified approach that refers to the battery equivalent circuits. The current is calculated according to Eq.3.2 [7].

$$I_{batt} = \frac{V_{batt,oc} - \sqrt{V_{batt,oc}^2 - 4R_b P_{batt}}}{2R_b} \tag{3.2}$$

where $V_{batt,oc}$ is the battery open circuit voltage, R_b the internal resistance and P_{batt} the power demanded.

At each time step the SOC state is updated using the previous current value flowing through the battery, according to 3.3.

$$SOC_{dev} = \frac{i_{batt}}{C_b 3600} \tag{3.3}$$

3.3.2 Fuel cell

As explained in [2] the polarization curve can be linearized, fitting the equation presented in Eq.3.4.

$$V_{fc}(t) = V_{fc,oc} - R_{fc} i_{fc}(t) \tag{3.4}$$

where $V_{fc,oc}$ represents the open-circuit voltage, i.e., the point at which the linearized voltage-current curve intersects the y-axis, so where $i_{fc} = 0$, and R_{fc} denotes the internal resistance, a value which is assumed constant for a given cell type under fixed operating conditions. In Fig.3.4 the linearized curve of the fuel cells is presented.

Eq. 3.4 represents the equivalent circuit model shown in Fig. 3.3 which characterizes the fuel cell system.

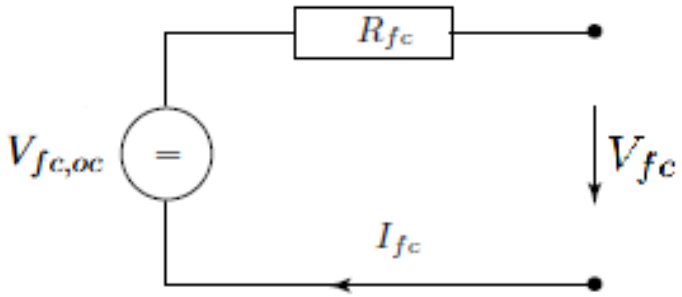

Figure 3.3. Fuel cell equivalent circuit used to model the system behaviour in the quasi static simulation.

The resulting current is calculated as shown in Eq.3.5, while at each time step the SOT is update following 3.6.

$$\dot{m}_{H_2} = \frac{M_{H_2} \cdot N_{\text{fc}} \cdot I_{\text{fc}}}{2F} = \frac{M_{H_2} \cdot N_{\text{fc}}}{2F} \cdot \frac{V_{fc,oc} - \sqrt{V_{fc,oc}^2 - 4R_{fc}P_{fc}}}{2R} \tag{3.5}$$

$$SOT_i = \frac{(SOT_{i-1} C_f - \dot{m}_{H_2})}{C_f} \tag{3.6}$$

where C_f is the capacity of full tank.

3.3.3 Drivetrain

The drivetrain model implemented in this study estimate the power demand required by the electric motor to propel the boat under various operational conditions. From the selected drag curve the drag force acting on the hull is evaluated. The total thrust required by the propeller is computed by summing the inertial force due to acceleration and the hydrodynamic drag resistance. Based on this required thrust, a dedicated function estimates the corresponding revolutions per minute (RPM) of the propeller using a simplified version of the fundamental propeller thrust equation (Eq. 3.7), which accounts for both geometric and hydrodynamic characteristics of the propeller.

$$T = K_T(\rho D^4 n^2), [n] = Hz \tag{3.7}$$

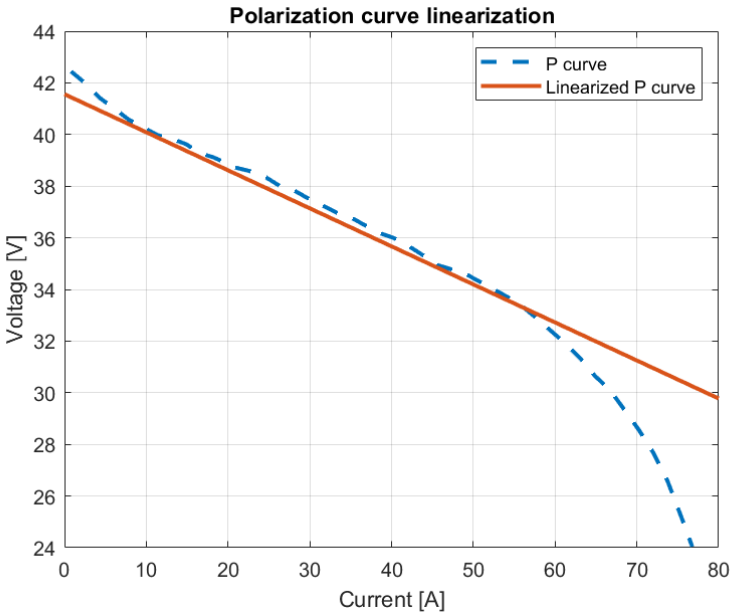

Figure 3.4. Fuel cell polarization curves: the one dotted taken by the fuel cell datasheet and the other made by linearization and used for the design phase.

As with the rotational speed, the required motor torque is estimated using a simplified form of the fundamental propeller torque equation (Eq. 3.8).

$$Q = K_Q(\rho D^5 n^2), [n] = Hz \tag{3.8}$$

The electric power required by the motor is finally calculated as shown in Eq.3.9.

$$P = \frac{Q \cdot \omega}{\eta_{em}} \tag{3.9}$$

In Fig. 3.5 the performance map of the motor is shown for completeness. This provides a realistic estimation of the power that must be delivered by the electric motor to achieve the desired motion, under the given environmental and dynamic constraints.

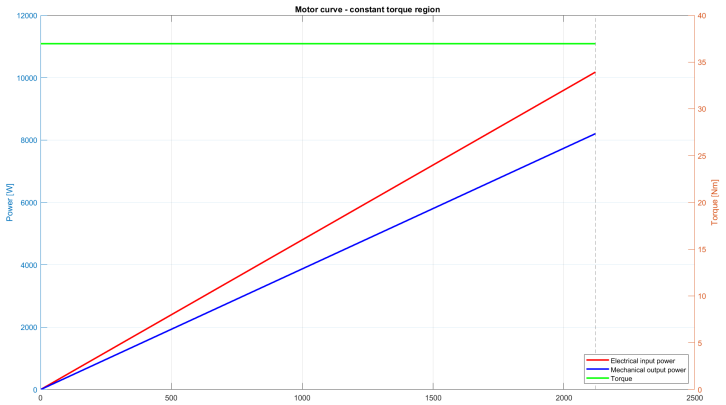

Figure 3.5. Motor performance map in constant torque region.

3.4 Bisection algorithm

The bisection method is a root-finding numerical algorithm that iteratively reduces the interval within which a function changes sign, thereby isolating the root. The method relies on the *Intermediate Value Theorem*, which states that if a continuous function $f(x)$ takes on opposite signs at two points a and b, then there exists at least one root $c \in (a, b)$ such that $f(c) = 0$. A schematic example is presented in Fig.3.6. This approach is known for its robustness and simplicity, offering guaranteed convergence under the condition that the initial interval brackets a root.

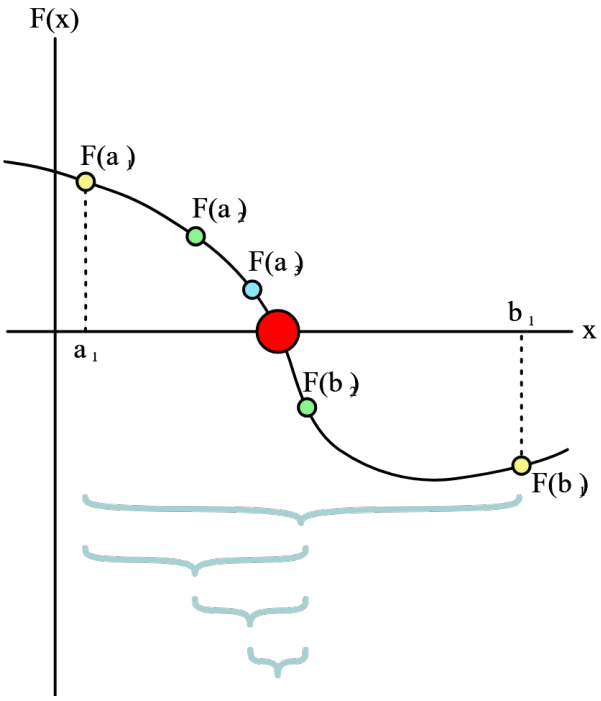

Figure 3.6. Graphical example of bisection algorithm procedure.

In the context of this study, the bisection algorithm is employed to optimize the energy management factor (λ) which governs the balance between battery and fuel cell power contributions. The goal is to minimize the deviation of the final state of charge (SOC) from a given reference at the end of a mission profile. Two extreme values for the equivalence factor are initially defined, representing scenarios of excessive battery discharge and under utilization, respectively. The SOC deviation corresponding to each extreme is simulated using the quasi-static model of the hybrid powertrain.

3.5 Controller design

The controller is designed through the optimization of the equivalent factor for each combination of drag and boat speed. For every pair of drag and speed values, a simulation is run over the defined mission, and a bisection method is used to iteratively determine the optimal eqFactor.

3.5.1 Mission definition

With respect to the endurance race, the mission on which the analysis is based, the objective is to optimize speed for minimal energy consumption and to maximize the number of laps completed. To achieve this, the range of constant speeds that the boat can ideally sustain is

discretized into 61 values, ranging from 4 knots to 19 knots. For each of these speed values, a corresponding mission profile is defined, resulting in 61 distinct speed profiles that can be simulated and evaluated. Based on these constant speed levels, perturbations are introduced to better represent real-world conditions and to enhance the robustness of the controller. An illustrative segment of a mission profile used for the controller design is shown in Fig.3.7.

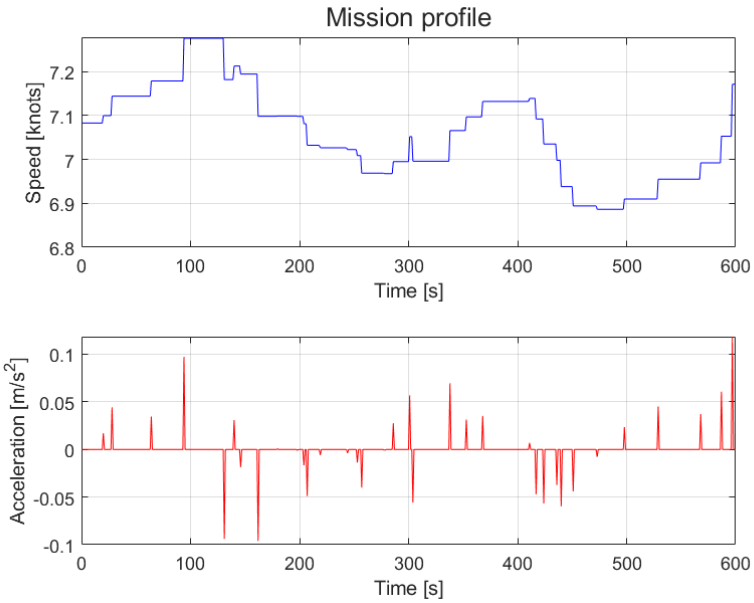

Figure 3.7. Mission profile based on constant speed of 7.2 knots. Time = 600s.

For each combination of drag condition and selected speed, an optimization is performed to determine the optimal equivalence factor (*eqFactor*) for the given scenario. The result is a 4 x 61 table containing the optimized *eqFactor* values for each pair of drag condition and speed.

The optimization is carried out using a bisection algorithm. The search interval for the equivalence factor is defined by the extremes 0.01 and 10, while the target final state of charge (SOC) is set to 0.2.

3.5.2 Results

Simulating all previously described cases, namely the four different drag conditions and 61 possible mission profiles, reveals that in many scenarios, it is not possible to identify an optimal equivalence factor. This typically occurs when the power demand is either too low, making it more efficient to keep the fuel cell turned off, or too high, requiring the fuel cell to operate at its nominal power. For clarity, Tab. 3.1 presents only the conditions in which the optimization successfully converged to an optimal value. The complete set of results, including the estimated number of laps at the end of the endurance race, is provided in Appendix 7.

Speed	Calm water	Low drag	Middle drag	High drag
8.35 knots	0.0100	0.0100	0.0100	0.0100
8.6 knots	0.0100	0.0100	0.0100	0.3222
8.85 knots	0.0100	0.0100	0.0100	0.3222
9.1 knots	0.0100	0.0100	0.0100	0.4002
9.35 knots	0.0100	0.0100	0.0100	0.4197
9.6 knots	0.0100	0.0100	0.0100	0.4393
9.85 knots	0.0100	0.0100	0.0100	0.4783
10.1 knots	0.0100	0.0100	0.4002	0.4978
10.35 knots	0.0100	0.0100	0.4197	0.5563
10.6 knots	0.0100	0.0100	0.4393	0.5050
10.85 knots	0.0100	0.0100	0.4393	10.0000
11.1 knots	0.0100	0.0100	0.5173	10.0000
11.35 knots	0.0100	0.0100	0.5173	10.0000
11.6 knots	0.0100	0.0100	0.5563	10.0000
11.85 knots	0.0100	0.0100	0.5954	10.0000
12.1 knots	0.0100	0.0100	0.5954	10.0000
12.35 knots	0.0100	0.3222	10.0000	10.0000
12.6 knots	0.0100	0.3222	10.0000	10.0000
12.85 knots	0.0100	0.3222	10.0000	10.0000
13.1 knots	0.0100	0.4197	10.0000	10.0000
13.35 knots	0.0100	0.4197	10.0000	10.0000
13.6 knots	0.0100	0.4393	10.0000	10.0000
13.85 knots	0.0100	0.4393	10.0000	10.0000
14.1 knots	0.0100	0.4783	10.0000	10.0000
14.35 knots	0.0100	0.4783	10.0000	10.0000
14.6 knots	0.0100	0.4783	10.0000	10.0000
14.85 knots	0.0100	0.5173	10.0000	10.0000
15.1 knots	0.0100	0.5954	10.0000	10.0000
15.35 knots	0.0100	0.5050	10.0000	0.0100
...	...	...	...	...
17.1 knots	0.3222	10.0000	0.0100	0.0100
17.35 knots	0.3222	10.0000	0.0100	0.0100
17.6 knots	0.3222	10.0000	0.0100	0.0100
17.85 knots	0.4002	10.0000	0.0100	0.0100
18.1 knots	0.4002	10.0000	0.0100	0.0100
18.35 knots	0.4197	10.0000	0.0100	0.0100
18.6 knots	0.4197	10.0000	0.0100	0.0100
18.85 knots	0.4393	10.0000	0.0100	0.0100
19.1 knots	0.4393	10.0000	0.0100	0.0100
19.35 knots	0.4588	10.0000	0.0100	0.0100
19.6 knots	0.4783	10.0000	0.0100	0.0100

Table 3.1. Equivalent factor results

Chapter 4

Simulation framework for the hybrid powertrain system

To accurately evaluate the behavior of the hybrid powertrain and assess the performance of the proposed control strategies, a dynamic simulation model was developed using MATLAB Simulink and Simscape [6]. The primary objective of this model is to provide a realistic representation of the system dynamics and to validate the control logic originally designed using a quasi-static approach. By comparing the outcomes of the quasi-static and dynamic simulations under the same race conditions, the effectiveness and robustness of the energy management strategy can be assessed. The expectation is that the dynamic model will yield results consistent with those obtained from the quasi-static model, thereby confirming the controller's validity in a more realistic simulation environment.

Considering the final application of the control system on the prototype, it is necessary to implement a fast routine capable of recognizing the drag condition closest to the design target, thereby allowing the system to automatically select the optimal configuration. This pattern recognizer has been implemented and is described in the following section. However, during computer simulation, it was bypassed by directly specifying constant sea conditions. In Fig.4.1 the role of the drag recognizer and the complete architecture of the implemented controller are illustrated in detail.

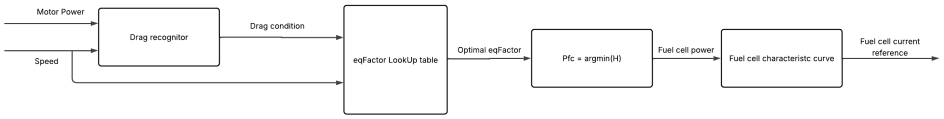

Figure 4.1. Energy management system overview.

4.1 Pattern recognition

In order for the system to autonomously adjust to the optimal design condition at any given moment, a software routine must run every x seconds to determine which of the four proposed drag conditions best represents the actual operating state.

Consequently, the recognitor to be implemented on board was designed in Simulink. The inputs to the system, whose Simulink block diagram is shown in Fig. 4.2, are the electrical power demanded by the electric motor, available via the CAN bus of the motor drivers, and the actual speed of the boat, acquired through onboard sensors.

The purpose of this block is to identify which drag curve best approximates the current environmental conditions.

Although the competition is held over a single day, there is a significant possibility that conditions may change during the 4-hour endurance race. The system is therefore designed to answer these variations, as well as other scenarios throughout the season when the boat may be in use, such as during test, exhibitions, or other competitions where the environmental condition can be different.

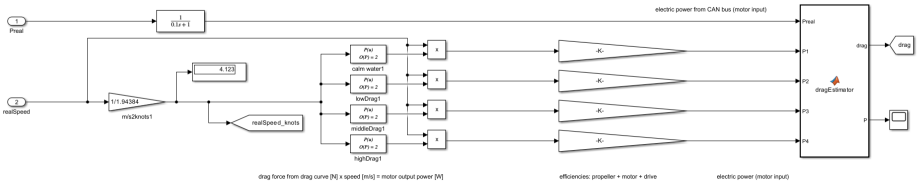

Figure 4.2. Pattern recognition block.

4.2 Powertrain model overview

The whole powertrain model is shown in Fig.4.3. It is divided into two main sections: the electrical and mechanical part.

On the electrical side, the energy sources, namely the battery and fuel cell, converge at a common DC bus that powers the electric motor. This electrical network is responsible for managing energy flow and supplying the required power to the propulsion system.

On the mechanical side, the system includes the driveline, which transmits torque from the motor shaft to the propeller. This latter models the dynamic interaction between the propulsion system and hydrodynamic resistance, accounting for drag forces acting on the vessel during operation.

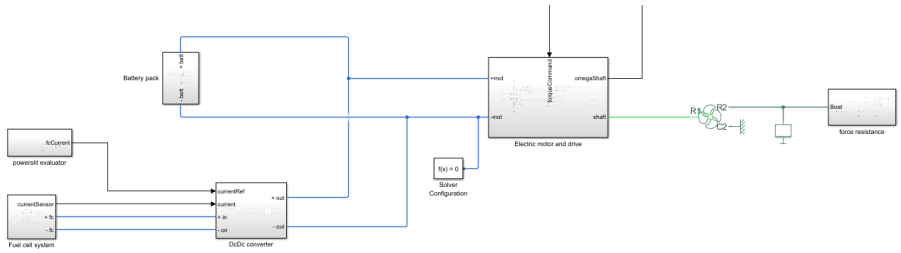

Figure 4.3. Hybrid powertrain model.

The battery is directly connected to the DC bus, while the fuel cell is interfaced through a unidirectional DCDC converter. For the purposes of this study, the converter is modeled using an average model controlled by a duty cycle (DC). The DCDC converter serves a dual purpose: first, to ensure that the input current drawn from the fuel cell closely matches the value determined by the control algorithm, the Equivalent Consumption Minimization Strategy (ECMS); second, to enable the connection of the fuel cell, which has a nominal output voltage of 28.8V, to the 48V DC bus.

It is important to note that the DC bus in this prototype is semi-regulated. This design choice was made to reduce the overall weight and cost of the onboard system. As a result,

the bus voltage is not actively controlled but instead varies depending on the battery's state of charge (SOC).

Considering the mechanical part of the model, the motor shaft block is connected both to the propeller block and to the hydrodynamic drag block representing the boat's resistance. The drag force is determined based on one of the four predefined drag curves, selected via a manual switch for simulation purpose.

Simultaneously, the thrust generated by the propeller is used to estimate the boat's speed. In this simulation setup, no sea currents are considered, neither in favor nor against the direction of motion. However, to incorporate such effects, it is sufficient to use the $R2$ port of the Simscape propeller block, as illustrated in Fig.4.4.

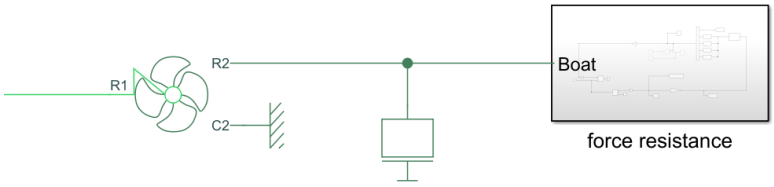

Figure 4.4. Propeller and resistance force block.

4.2.1 Fuel cell and battery hybridization review

Generally speaking, the fuel cell battery hybridization architecture can be chosen among different connection methods [9]. For this type of configuration, four main approaches are commonly adopted, distinguished by the number and function of DCDC converters used.

The first configuration is the direct connection of dual-energy sources, where both the fuel cell system and the battery are connected directly to the DC bus without any DCDC converter. This setup is simple and cost-effective but suffers from significant drawbacks: the bus voltage is highly sensitive to load changes, leading to potential voltage fluctuations and reduced system controllability.

In the second approach, direct connection of the FCS, the fuel cell is directly connected to the DC bus, while the battery is linked through a bidirectional DCDC converter. This enables better control of battery power flow and allows for batteries with lower voltage ratings. However, since the FC sets the bus voltage, any variation in fuel cell power leads to substantial voltage fluctuations, potentially undermining system stability and performance.

The third option is the direct connection of the battery, shown in Fig.4.5, where the battery is connected directly to the DC bus and the FC via a unidirectional DCDC converter. This setup lowers stress on the fuel cell by smoothing power demands, improving fuel cell efficiency and life. Nonetheless, the systems voltage entirely depends on the battery's state-of-charge.

Finally, the most flexible but complex configuration is the indirect connection of dual-energy sources, where both the FC and the battery are interfaced with the DC bus via dedicated converters. This arrangement improves control over energy flows and stabilizes the bus voltage, regardless of fluctuations in either source. However, it comes at the cost of greater spatial requirements, higher component costs, reduced efficiency, and the need for larger filter capacitors due to increased ripple currents.

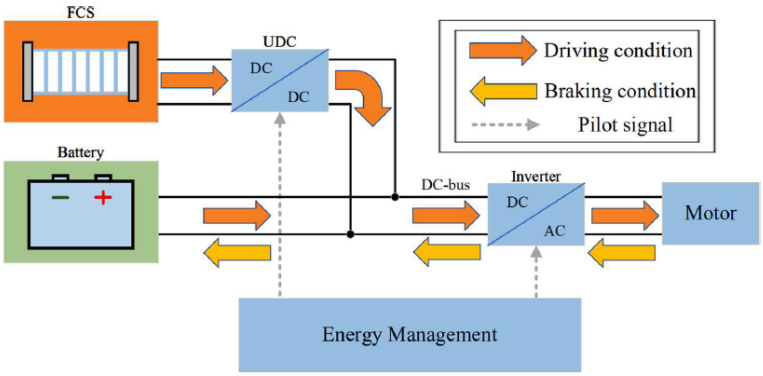

Figure 4.5. Direct parallel connection of the battery [9]. The solution adopted in the powertrain in analysis.

4.2.2 Battery system block

The battery block is implemented using an equivalent circuit consisting of a variable DC voltage source and an internal variable resistance. Both values are defined as functions of the state of charge (SOC) to accurately replicate the real battery behavior. The implemented block is shown in Fig.4.6. The output of the block are the positive and negative terminals of the battery.

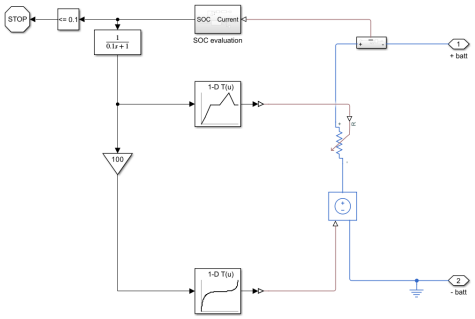

Figure 4.6. Battery block.

4.2.3 Motor and drive system block

For the purpose of this study, it is enough to use a dedicated motor and drive block, from Simscape library, that simulates the behavior of the electric motor and its driver. The block receives the demanded torque as input and outputs both electrical signals, connected to the DC bus, and mechanical signal, connected to the propeller, as illustrated in Fig. 4.7.

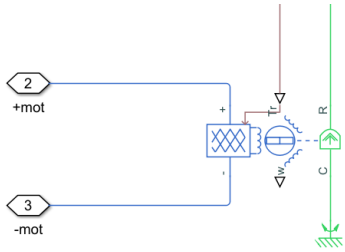

Figure 4.7. Motor and Drive block.

4.2.4 Fuel cell system block

A simplified fuel cell system is considered, in which dynamic behavior is neglected. The Nernst voltage is computed under nominal temperature and pressure conditions. All the parameters are directly extracted from the characteristic graphs provided in the datasheet of the fuel cell used. The fundamental equations used to model the system are based on [5], while the implemented block is shown in Fig. 4.8.

$$E = E_{FC,oc} - NA \ln\left(\frac{i_{FC}}{i_0}\right) \tag{4.1}$$

$$v_{FC} = N_{unit}E - R_i i_{FC} - v_d \tag{4.2}$$

$$\frac{1}{R_d}\left(\tau\frac{dv_d}{dt} + v_d\right) = i_{FC} \tag{4.3}$$

In these equations, E_{oc} represents the open-circuit voltage, v_{FC} is the voltage across the fuel cell terminals, A denotes the Tafel slope, and $\tau = R_d C_{dl}$ is the time constant. The Tafel slope A is defined by trial end error in order to keep the fuel cell model results the most similar to the one provided in the datasheet.

Figure 4.8. Fuel cell block.

4.2.5 DCDC converter system block

The high fidelity of the DCDC converter model is not required for the purposes of this study. Therefore, an average DCDC converter block is adopted. The converter is controlled via a duty cycle signal, which is modulated to ensure that the input current drawn from the fuel cell matches the reference current set by the ECMS (Equivalent Consumption Minimization Strategy). In this model, no closed-loop control is implemented for the DC bus voltage, which instead results from the balance between the battery voltage and the output voltage of the DC/DC converter. The implemented DCDC converter and its control scheme are shown in Fig.4.9. The purpose of the DCDC converter is to maintain power continuity, net of the component's efficiency, between its input and output while allowing modulation of voltage and current levels.

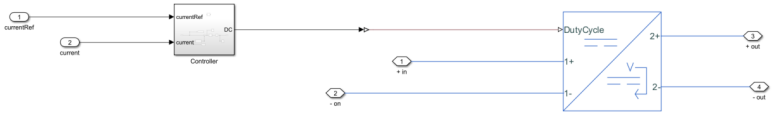

Figure 4.9. DCDC converter block.

4.2.6 Propeller block

The propeller is modeled using the Simscape Propeller block, where specific parameters such as diameter, torque coefficient, and thrust coefficient of the endurance propeller are configured. This block converts rotational mechanical energy at the shaft into linear force, producing the thrust exploited for propulsion. The fundamental equations governing the propeller behavior are:

$$T = k_T \rho D_n^4 \, n \sqrt{n^2 + n_{\text{thr}}^2} \tag{4.4}$$

$$Q = k_Q \rho D_n^5 \, n \sqrt{n^2 + n_{\text{thr}}^2} \tag{4.5}$$

4.2.7 Drag evaluation block

In the simulation model, drag is computed using a dedicated block directly integrated into the physical system, reported in Fig.4.10 and Fig.4.11. Specifically, at the translational input of the propeller, a drag force is applied in addition to the inertial mass. This force is proportional to the velocity and follows one of the predefined drag curves, which are selected based on the simulated sea conditions.

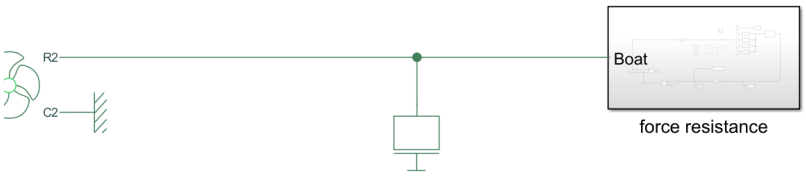

Figure 4.10. Drag evaluation block connection.

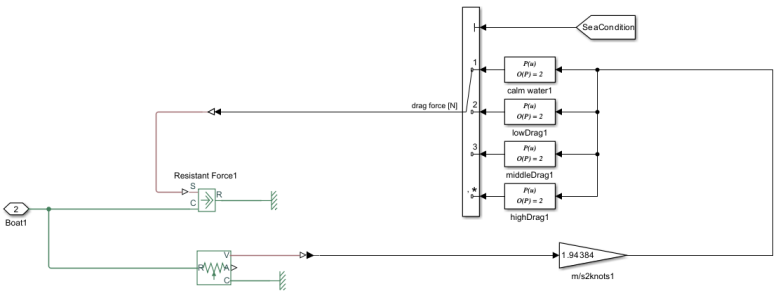

Figure 4.11. Drag evaluation block.

4.3 Driver model and torque controller

In the context of a simulation of the race, it is necessary to define a system that replaces the human driver and take the decision about throttle behaviour. For this purpose, a driver model, shown in Fig.4.12, has been developed. This block reads both the reference speed and the actual speed of the boat to generate a throttle command, ranging from 0 to 1. The used model is part

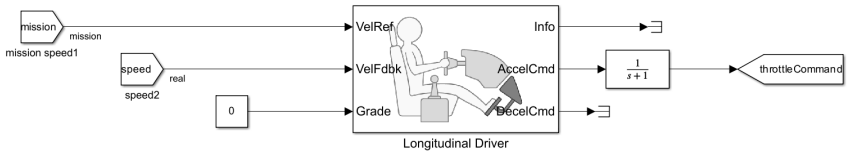

Figure 4.12. Driver model block.

of automotive toolbox, where the road grade is set to 0, avoiding the influence of it and the deceleration output is not considered.

Once the throttle input, expressed as a percentage of the boats actual throttle, is determined, it needs to be converted into a torque command for the motor. To achieve this, a torque controller has been implemented. This controller regulates the required torque based on the difference between the desired and actual angular speeds of the motor shaft. The reference angular speed is obtained by interpolating a predefined speed curve as a function of the throttle input. The complete torque control model is illustrated in Fig.4.13.

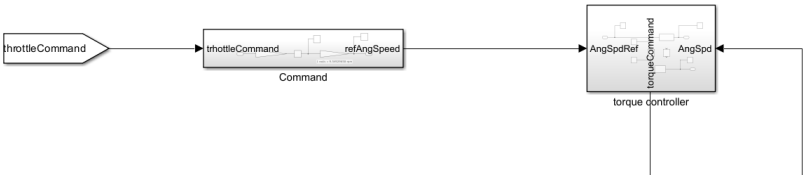

Figure 4.13. Torque controller block.

4.4 Controller integration

The controller is implemented using a lookup table, which selects the pre-evaluated equivalence factor based on the recognized drag condition and the current speed from the simulation, provided as an input to the block. Once the appropriate equivalence factor is selected, the fuel cell power output (P_{fc}) is computed using the analytical formulation of the Equivalent Consumption Minimization Strategy (ECMS), Eq:4.6.

$$P_{fc} = \frac{-3240000\mu 1 V_b^2 + 12960000 P_d R_b \mu 1 + F^2 V_{fc}^2 s^2}{4(3240000 R_b \mu 1 + R_{fc} F^2 s^2)} \tag{4.6}$$

with

$$\mu 1 = C_b^2 M^2 N^2 \tag{4.7}$$

Then, referring to the fuel cells power versus current characteristic curve, shown in Fig.4.14, the corresponding current required from the fuel cell is determined and provided as output of the block. This current is subsequently used as the reference input for the control of the DC-DC converter.

The complete controller implementation is reported in Fig.4.15 and Fig.4.16.

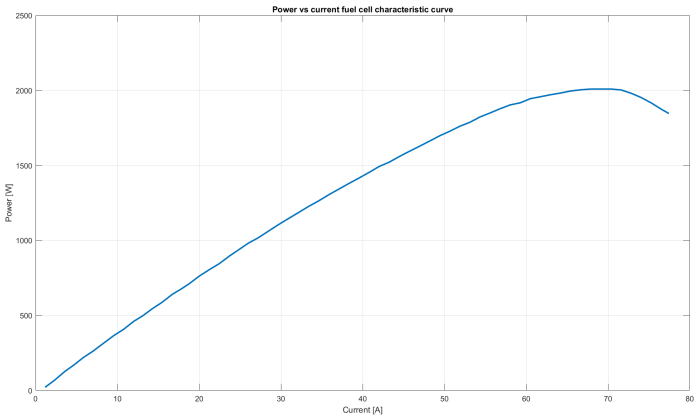

Figure 4.14. Power vs current characteristic curve of the fuel cell.

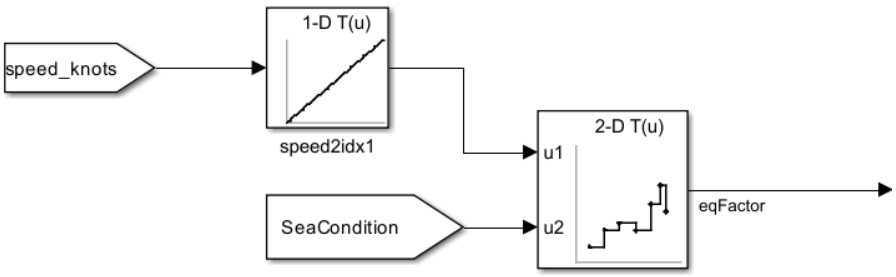

Figure 4.15. Controller LookUp table. Input: drag condition and speed. Output: eqFactor.

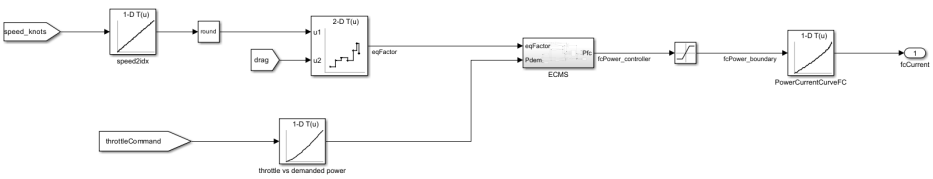

Figure 4.16. ECMS controller implementation in simulation framework.

Chapter 5

Simulation results and performance evaluation

Since the goal of this study is to develop a controller that optimizes performance during the endurance race, the results for three representative operating conditions are presented below:

- **Low power demand**, meaning low speed and/or low hull drag: the optimal strategy in this case is to keep the fuel cell off and supply all the required power from the battery. This effectively turns the vehicle into a battery electric vehicle (BEV), as hydrogen is not used. Additionally, by not operating the fuel cell, the system avoids frequent load variations or an ON/OFF behavior on it, which would be detrimental to efficiency and durability of the cell.
- **High power demand**, meaning high speed and/or high drag: this represents a critical situation for the powertrain. The required power is so high that the strategy is to operate the fuel cell at its nominal power output continuously, while the battery provides the remaining power. This condition results in higher hydrogen consumption, but the fuel cell operates within a high-efficiency region.
- **Medium power demand**: in this intermediate case, the optimization strategy can split the power between the two energy sources. The goal here is to minimize hydrogen consumption while maintaining a steady fuel cell output for an extended period, thereby improving overall efficiency and prolonging fuel cell life.

In the following section, representative results for the three operating conditions are presented, with a focus on the intermediate-range scenario in which the optimal strategy provides significant performance improvements. The controller, developed based on a quasi-static optimization approach, is validated through a dynamic simulation that emulates realistic operating conditions.

5.1 Design validation

The results shown in Fig. 5.1 and Fig.5.2 illustrate a close agreement between the quasi-static design and the dynamic simulation. The State of Charge (SOC) and State of Tank (SOT) exhibit a gradual decrease over time, with the dynamic simulation closely following the trends observed in the design phase. Minor discrepancies, particularly in the later stages of the simulation, can be attributed to dynamic effects not captured by the static model and to the discretization of the battery power during the design phase. The power distribution among the motor, battery, and fuel cell also confirms the strategy: while the design uses a load-following profile for the fuel cell, the dynamic simulation implements a smoother fuel cell power trajectory, reporting

transient demands to the battery. Additionally, the control variable differs between the design and simulation phases; in the real-world application considering the hybrid architecture, direct parallel connection of the battery, it is more practical to regulate the fuel cell using a reference current rather than regulate a power absorbed by the battery as done in design phase. This effectively reduces high-frequency load fluctuations on the fuel cell, fuel cell current is stabilized, mitigating potential degradation and performance over time. These results confirm that the controller successfully manages the power flow under real dynamic conditions, validating the initial quasi-static optimization. The operating conditions used in the simulations are reported in Tab.5.3.

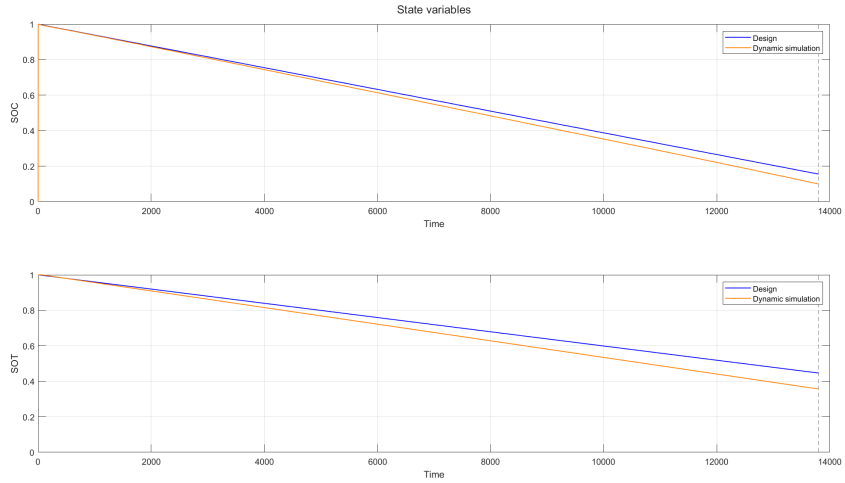

Figure 5.1. State variables in design and simulation phase.

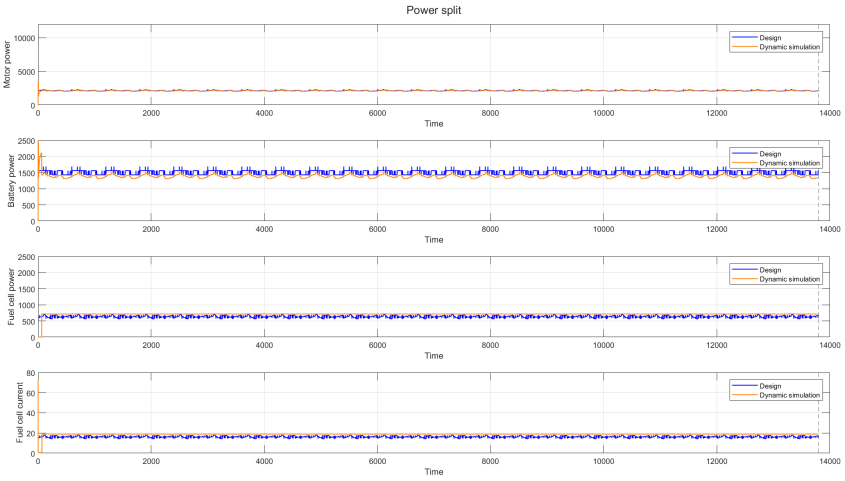

Figure 5.2. Power split in design and simulation phase.

5.2 Low power operating condition

The simulation conditions for the low power demand scenario are summarized in Tab.5.1.

Fig.5.4 presents the results obtained from the dynamic model over the endurance race.

Speed	8.1 knots
Drag	2 (lowDrag)
eqFactor	0.01

Table 5.1. Low power operating condition.

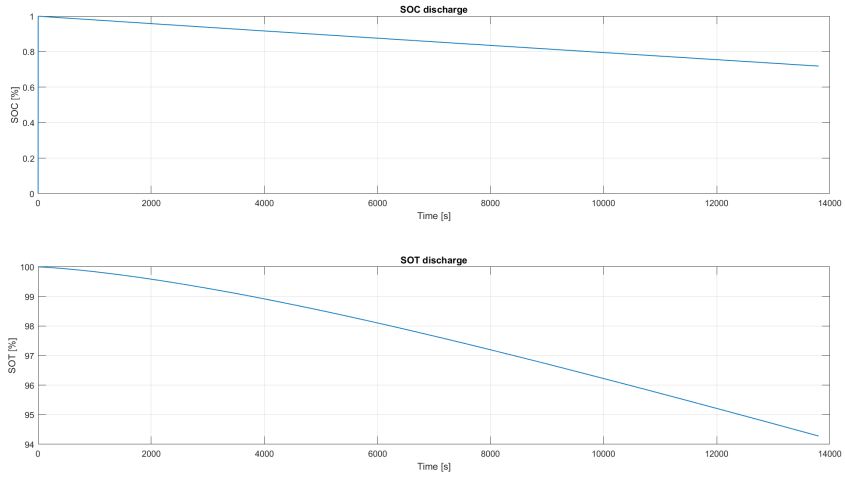

Figure 5.3. SOC and SOT discharge - low power operating condition.

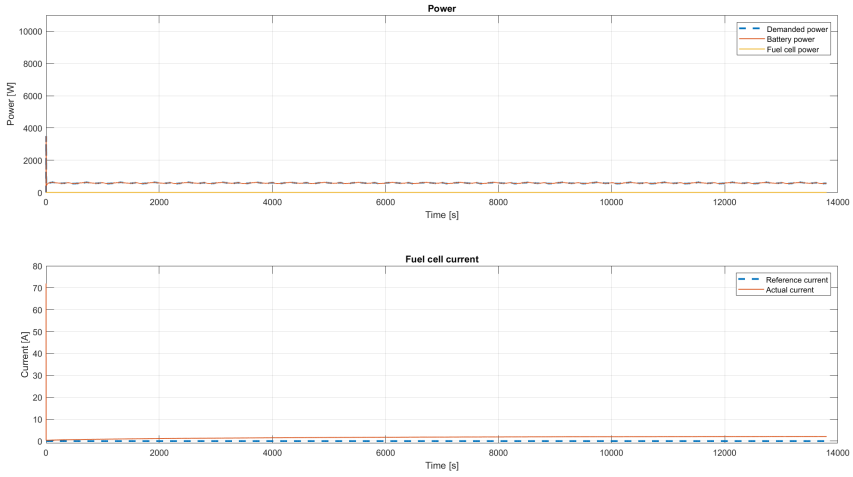

Figure 5.4. Power and current curve - low power operating condition.

5.3 High power operating condition

The configuration parameters corresponding to the high-power demand scenario are presented in Tab.5.2. Fig.5.6 shows the system configuration and the dynamic model's performance over the course of the endurance race.

Speed	17.6 knots
Drag	2 (lowDrag)
eqFactor	10.00

Table 5.2. High power operating condition.

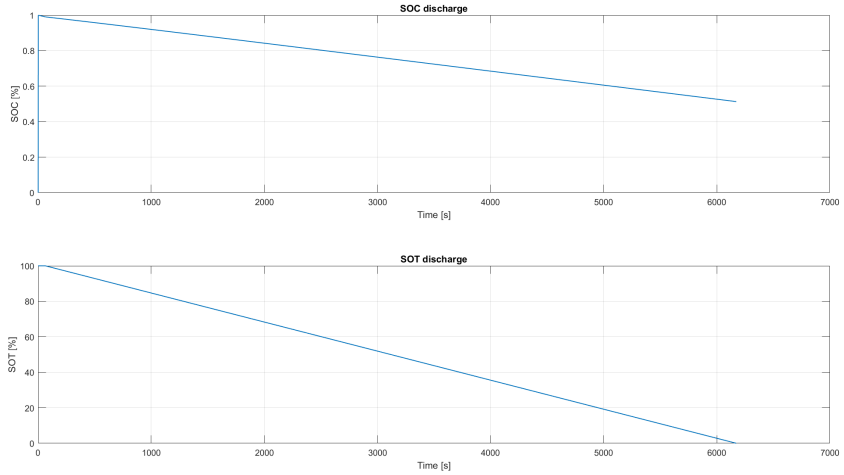

Figure 5.5. SOC and SOT discharge - high power operating condition.

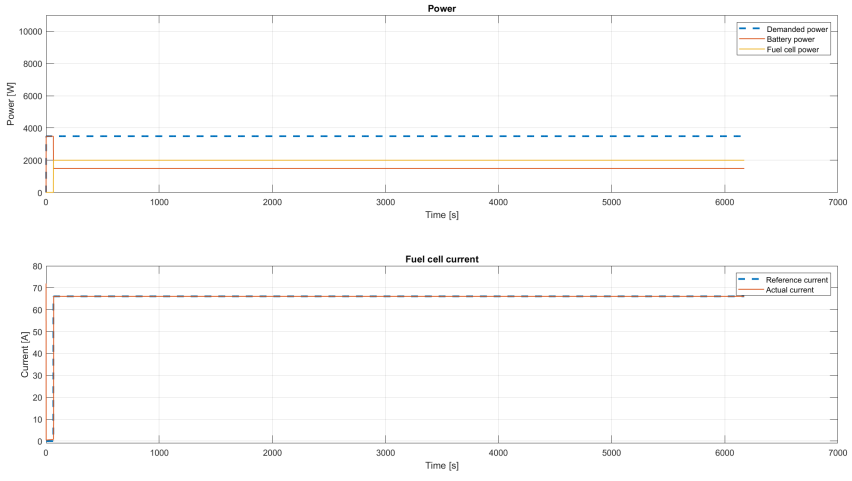

Figure 5.6. Power and current curve - high power operating condition.

5.4 Middle power operating condition

In this section, the behavior of the powertrain under medium power demand is analyzed, focusing on how energy is efficiently distributed between the available sources. All the consideration are based on an example simulation, whose condition are reported in Tab.5.3.

5.4.1 Powersplit

For the intermediate power range, the optimization is achieved by distributing the power demand between the battery pack and the fuel cell. The corresponding results are presented in Fig.5.8 and Fig.5.9.

Speed	12.58 knots
Drag	2 (lowDrag)
eqFactor	0.342

Table 5.3. Operation point with optimal eqFactor

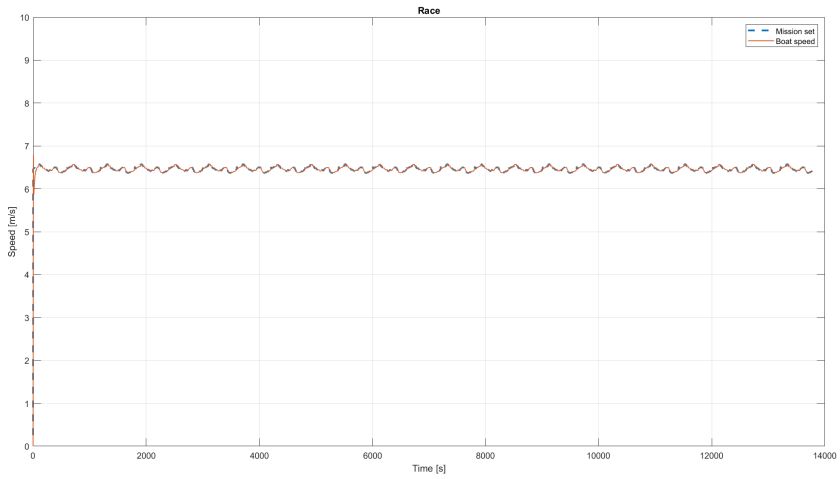

Figure 5.7. Boat speed during the simulation

The simulation results also confirm that the boat successfully reaches and sustains the desired speed, as illustrated in Fig.5.7.

For completeness, and with respect to the original optimization goal, the simulation results in a total of 16 completed laps.

5.4.2 Endurance race simulation results

Based on the work done for the competition, this section evaluates the benefits of using the optimized control strategy during the endurance race. To do this, three different simulations are compared: one using the optimized power split (Optimal mode), one with the fuel cell turned off (battery mode), and one with the fuel cell always operating at maximum power (FullFC mode). The results are summarized in Tab.5.4, and the behavior of the main state variables is shown in Fig.5.11, Fig.5.13 and Fig.5.15.

It should be noted that the simulation stops if the battery state of charge (SOC) drops below 0.2. In this case, the fuel cell alone cannot provide enough power to operate the system safely or, depending on the sea conditions, following the rules defined by the competition.

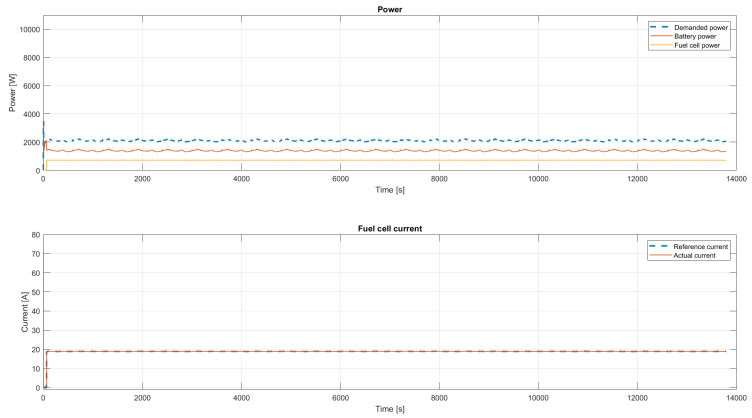

Figure 5.8. Power distribution and fuel cell current.

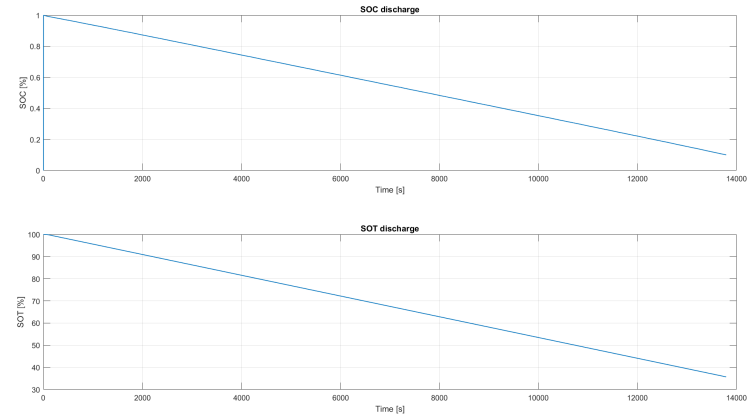

Figure 5.9. State variable.

Mode	Completed laps	Theoretical laps	Final SOC [%]	Final SOT [%]
Optimal	14	14.31	20	42.64
Battery	10	10.39	20	95.02
FullFC	unfeasible	16.04	92	-139.33
FullFC *	6	6.7	96	0

Table 5.4. Completed laps during a full endurance race simulation.

* The simulation is stopped when the SOT reaches zero, resulting in a total runtime of only 1 hour and 36 minutes.

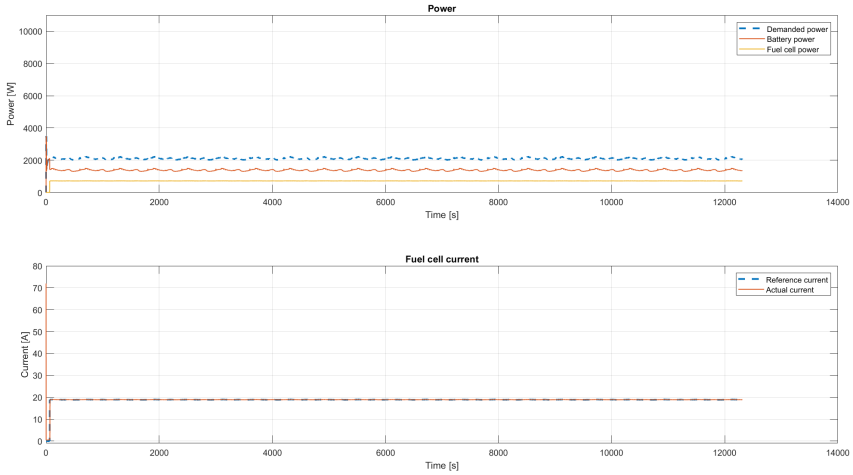

Figure 5.10. Optimal mode: power distribution. The current is maintained close to the reference value, correctly dividing the power between the two energy sources.

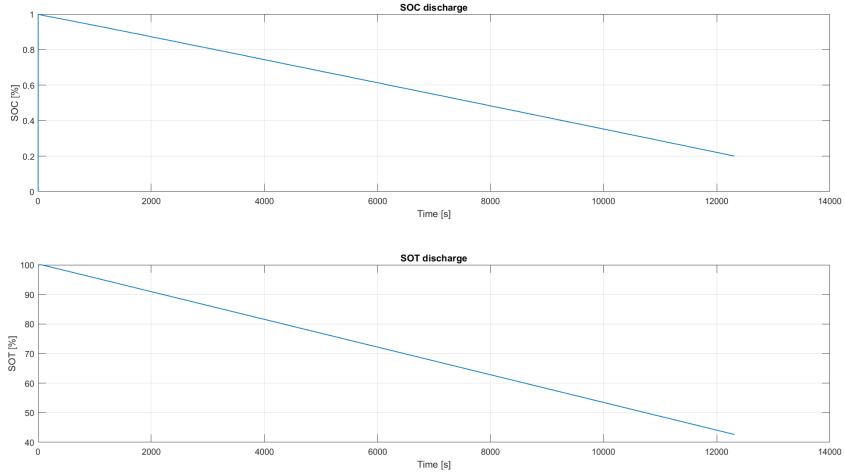

Figure 5.11. Optimal mode: state variable. The SOC is gradually discharged throughout the race, enabling the battery to handle peak power demands. Meanwhile, the fuel cell provides a stable base power level. Further analysis could suggests that hydrogen could be utilized more extensively, as the SOT does not reach 0% by the end of the race. This is justified by the absence of a predefined target SOC value at the race conclusion in the controller design.

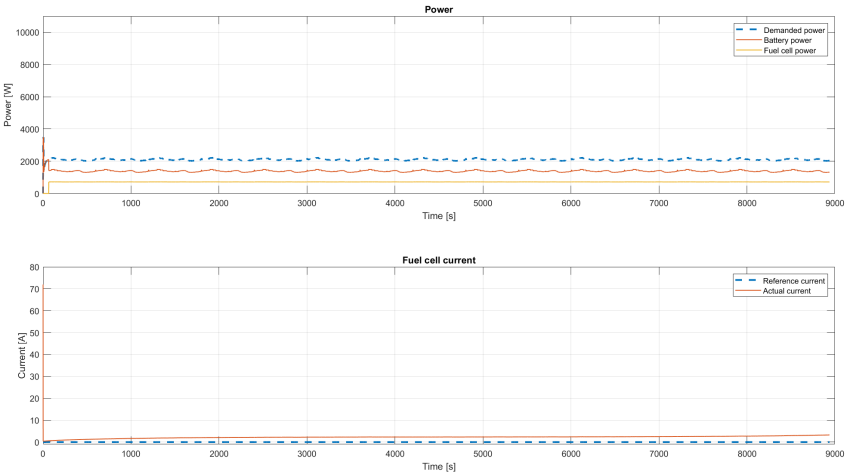

Figure 5.12. Battery only mode: power distribution.

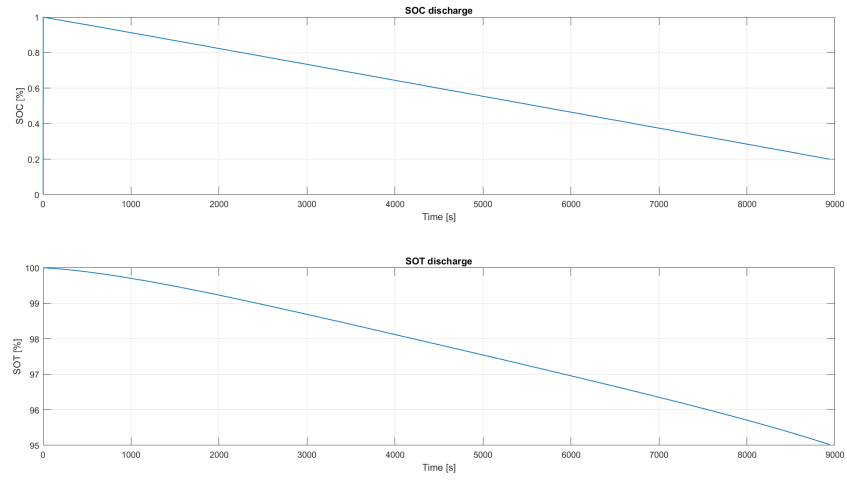

Figure 5.13. Battery only mode: state variable.

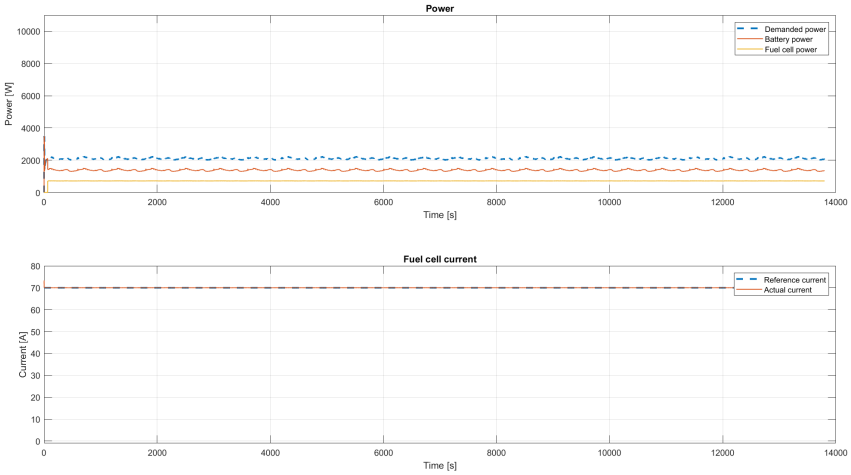

Figure 5.14. Fuel cell at maximum power mode: power distribution.

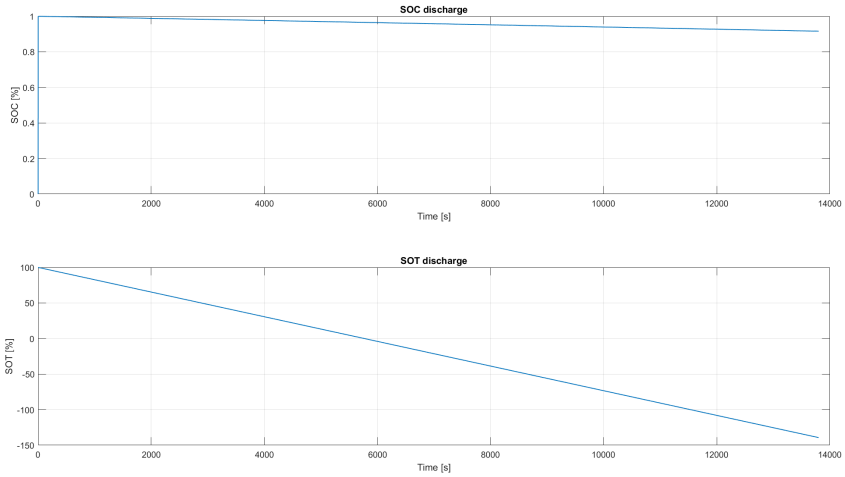

Figure 5.15. Fuel cell at maximum power mode: state variable. The SOT drops to zero quickly, resulting in the powertrain operating solely on the battery for the remainder of the race, without benefiting from any optimization strategy.

Chapter 6

Conclusion

This thesis aimed to develop and validate an energy management strategy for a hybrid powertrain system integrating a hydrogen fuel cell and a lithium-ion battery, with particular focus on the endurance race of the competition. Motivated by the favorable energy weighting of hydrogen and the system's potential to exceed the nominal efficiency threshold of 40%, the work focused on optimizing the energy distribution between the two power sources to enhance overall performance and extend operational range.

To address this objective, a two-phase workflow was implemented. First, a quasi-static optimization was carried out to determine the optimal equivalent factor (eqFactor) values for different propulsion scenarios. These values were then used to build a control strategy capable of dynamically adapting to varying power demands. In the second phase, the strategy was tested and validated through simulations using a detailed Simscape model of the powertrain, which accurately reproduced the dynamics of the real system.

The results demonstrated the effectiveness of the proposed EMS in achieving a balanced and efficient distribution of power between the battery and fuel cell, particularly under endurance conditions. The controller was able to respond appropriately to different speed profiles and maintain system operability even under different demanding load requirements. These findings validate the initial hypothesis that a well-designed hybrid control strategy can significantly increase the usable energy from hydrogen under competition constraints, ultimately enhancing the prototype's autonomy and performance.

6.1 Further investigations and improvements

Because this study represents a preliminary analysis aimed at the implementation and optimization of a hybrid energy system, several future developments, both direct and related, can be pursued to enhance the system's effectiveness and integration. The most relevant opportunities, particularly in relation to the evolution of the race prototype, include the following.

- Expand the management software by developing dedicated control maps for the other race formats (e.g., slalom, sprint, championship), where full optimization may not be the primary objective, but reliable and responsive powertrain control remains essential.
- Testing and simulation of the system using dedicated hardware, allowing validation of the control strategies under realistic operating conditions;
- Progressive refinement of the design tool by integrating increasingly accurate data collected during dedicated test sessions and real competition scenarios, such as drag conditions, speed targets, and propeller RPMs;
- Design and/or selection of a dedicated DCDC converter, capable of enabling precise control of the fuel cell load. This would allow for the definition of a target current request, making

it possible to fully exploit the fuel cell's and optimization potential within the hybrid system architecture.

These future steps aim not only to close the gap between simulation and reality, but also to support a more robust and adaptable energy management strategy.

Chapter 7

Appendix A: Optimization results

7.1 Optimized equivalent factor results

Speed (knots)	Calm water	Low drag	Middle drag	High drag
4.6 knots	0.01	0.01	0.01	0.01
4.85 knots	0.01	0.01	0.01	0.01
5.1 knots	0.01	0.01	0.01	0.01
5.35 knots	0.01	0.01	0.01	0.01
5.6 knots	0.01	0.01	0.01	0.01
5.85 knots	0.01	0.01	0.01	0.01
6.1 knots	0.01	0.01	0.01	0.01
6.35 knots	0.01	0.01	0.01	0.01
6.6 knots	0.01	0.01	0.01	0.01
6.85 knots	0.01	0.01	0.01	0.01
7.1 knots	0.01	0.01	0.01	0.01
7.35 knots	0.01	0.01	0.01	0.01
7.6 knots	0.01	0.01	0.01	0.01
7.85 knots	0.01	0.01	0.01	0.01
8.1 knots	0.01	0.01	0.01	0.17
8.35 knots	0.01	0.01	0.01	0.32
8.6 knots	0.01	0.01	0.01	0.34
8.85 knots	0.01	0.01	0.01	0.35
9.1 knots	0.01	0.01	0.32	0.36
9.35 knots	0.01	0.01	0.32	0.38
9.6 knots	0.01	0.01	0.34	0.40
9.85 knots	0.01	0.01	0.34	0.44
10.1 knots	0.01	0.01	0.36	0.48
10.35 knots	0.01	0.01	0.38	5.00
10.6 knots	0.01	0.01	0.40	10.00
10.85 knots	0.01	0.01	0.42	10.00
11.1 knots	0.01	0.01	0.44	10.00
11.35 knots	0.01	0.01	0.48	10.00
11.6 knots	0.01	0.32	5.00	10.00
11.85 knots	0.01	0.32	10.00	10.00
12.1 knots	0.01	0.33	10.00	10.00
12.35 knots	0.01	0.34	10.00	10.00

Next page...

Speed (knots)	Calm water	Low drag	Middle drag	High drag
12.6 knots	0.01	0.34	10.00	10.00
12.85 knots	0.01	0.36	10.00	10.00
13.1 knots	0.01	0.38	10.00	10.00
13.35 knots	0.01	0.38	10.00	10.00
13.6 knots	0.01	0.40	10.00	10.00
13.85 knots	0.01	0.42	10.00	10.00
14.1 knots	0.01	0.44	10.00	10.00
14.35 knots	0.01	0.48	10.00	10.00
14.6 knots	0.01	5.00	10.00	10.00
14.85 knots	0.01	10.00	10.00	10.00
15.1 knots	0.01	10.00	10.00	10.00
15.35 knots	0.01	10.00	10.00	0.01
15.6 knots	0.01	10.00	10.00	0.01
15.85 knots	0.01	10.00	10.00	0.01
16.1 knots	0.17	10.00	10.00	0.01
16.35 knots	0.32	10.00	10.00	0.01
16.6 knots	0.32	10.00	10.00	0.01
16.85 knots	0.33	10.00	10.00	0.01
17.1 knots	0.34	10.00	0.32	0.01
17.35 knots	0.34	10.00	0.01	0.01
17.6 knots	0.35	10.00	0.01	0.01
17.85 knots	0.36	10.00	0.01	0.01
18.1 knots	0.36	10.00	0.01	0.01
18.35 knots	0.38	10.00	0.01	0.01
18.6 knots	0.38	10.00	0.01	0.01
18.85 knots	0.40	10.00	0.01	0.01
19.1 knots	0.42	10.00	0.01	0.01
19.35 knots	0.44	10.00	0.01	0.01
19.6 knots	0.44	10.00	0.01	0.01

7.2 Endurance lap results

Speed (knots)	Calm water	Low drag	Middle drag	High drag
4.6 knots	5.82	5.82	5.82	5.82
4.85 knots	6.14	6.14	6.14	6.14
5.1 knots	6.46	6.46	6.46	6.46
5.35 knots	6.78	6.78	6.78	6.78
5.6 knots	7.10	7.10	7.10	7.10
5.85 knots	7.42	7.42	7.42	7.42
6.1 knots	7.74	7.74	7.74	7.74
6.35 knots	8.06	8.06	8.06	8.06
6.6 knots	8.38	8.38	8.38	8.38
6.85 knots	8.70	8.70	8.70	8.70
7.1 knots	9.02	9.02	9.02	9.02
7.35 knots	9.34	9.34	9.34	9.34
7.6 knots	9.66	9.66	9.66	9.66
7.85 knots	9.98	9.98	9.98	9.98
8.1 knots	10.30	10.30	10.30	10.30
8.35 knots	10.62	10.62	10.62	10.62
8.6 knots	10.93	10.93	10.93	10.93
8.85 knots	11.25	11.25	11.25	11.25
9.1 knots	11.57	11.57	11.57	11.57
9.35 knots	11.89	11.89	11.89	11.89
9.6 knots	12.21	12.21	12.21	12.21
9.85 knots	12.53	12.53	12.53	12.53
10.1 knots	12.85	12.85	12.85	12.85
10.35 knots	13.17	13.17	13.17	13.17
10.6 knots	13.49	13.49	13.49	13.49
10.85 knots	13.81	13.81	13.81	13.81
11.1 knots	14.13	14.13	14.13	14.13
11.35 knots	14.45	14.45	14.45	14.45
11.6 knots	14.77	14.77	14.77	14.77
11.85 knots	15.09	15.09	15.09	15.09
12.1 knots	15.41	15.41	15.41	15.41
12.35 knots	15.73	15.73	15.73	15.73
12.6 knots	16.05	16.05	16.05	16.05
12.85 knots	16.36	16.36	16.36	16.36
13.1 knots	16.68	16.68	16.68	16.68
13.35 knots	17.00	17.00	17.00	17.00
13.6 knots	17.32	17.32	17.32	17.32
13.85 knots	17.64	17.64	17.64	17.64
14.1 knots	17.96	17.96	17.96	17.96
14.35 knots	18.28	18.28	18.28	18.28
14.6 knots	18.60	18.60	18.60	18.60
14.85 knots	18.92	18.92	18.92	18.92
15.1 knots	19.24	19.24	19.24	19.24
15.35 knots	19.56	19.56	19.56	19.56
15.6 knots	19.88	19.88	19.88	19.88

Next page...

Speed (knots)	**Calm water**	**Low drag**	**Middle drag**	**High drag**
15.85 knots	20.20	20.20	20.20	20.20
16.1 knots	20.52	20.52	20.52	20.52
16.35 knots	20.84	20.84	20.84	20.84
16.6 knots	21.16	21.16	21.16	21.16
16.85 knots	21.48	21.48	21.48	21.48
17.1 knots	21.80	21.80	21.80	21.80
17.35 knots	22.11	22.11	22.11	22.11
17.6 knots	22.43	22.43	22.43	22.43
17.85 knots	22.75	22.75	22.75	22.75
18.1 knots	23.07	23.07	23.07	23.07
18.35 knots	23.39	23.39	23.39	23.39
18.6 knots	23.71	23.71	23.71	23.71
18.85 knots	24.03	24.03	24.03	24.03
19.1 knots	24.35	24.35	24.35	24.35
19.35 knots	24.67	24.67	24.67	24.67
19.6 knots	24.99	24.99	24.99	24.99

Chapter 8

Appendix B: MATLAB script

8.1 Quasi static powertrain model

```
function [x_next,h2_flow_rate,unfeas,motorPower,fcPower,battCurrent,fcCurrent,...
    outboardLimit] = powertrain_model(x,u,w, batt,fc,em, boatData,tank, ...
    dragCurve,propeller)

%% -- Input --
% x: State vector
% u: Control vector
% w: Exogenous input vector
% batt, fc, em, boatData: structures containing data

%% --Output--
% x_next: next state of the system
% cost: coste of the stage
% unfeas: indicate some kind of constraint violation
% motorPower
% fcPower

%% -- Model details --
% State variables
%   x(1)    Battery SOC,
%   x(2)    State of Tank
% Control variables
%   u(1)    Battery Power
% Exogenous inputs
%   w(1)    Boat speed, m/s
%   w(2)    Boat acceleration, m/s^2

dt = 1;

%% --- Evaluation --- %%

[motorTrq,rpm,outboardLimit] = ...
    drivetrain_model(w(1),w(2),boatData,dragCurve,propeller);

shaftSpeed = rpm/9.54929658;
```

```
% Electric power consumption
motorPower = shaftSpeed .*motorTrq ./(em.etaTest/100);

%% Battery

battCurrent = (Voc - sqrt(Voc^2 - 4*R0.*u{1}))./2./R0;
battCurrent = real(battCurrent);

% SOC dynamic
SOC_dev = battCurrent./Q_nom/3600 .*dt;
SOC_next = SOC - SOC_dev;

%% Motor
motorPower = repmat(motorPower, 1, numel(battCurrent));

%% DcDc converter
etaDcDC = 0.98;
fcPower = (motorPower - u{1})./etaDcDC;

%% Fuel cell
fcCurrent = (fc.Voc - sqrt(fc.Voc^2 - 4*fc.R.*fcPower))./2./fc.R;

h2_flow_rate = fc.M*fc.Ncell*fcCurrent/(2*fc.F);

%% State Of Tank (SOT) dynamic
SOT_next = (SOT*tank.fullTankCapacity - h2_flow_rate)/tank.fullTankCapacity;

x_next = [SOC_next' SOT_next'];


%% Unfeasibility due to components
% Battery
battUnfeas = (battCurrent > iMaxDischarge);

% Motor
motorUnfeas = (motorPower > emPowerMax);

% Fuel cell
fcUnfeas = (fcPower > fcPowerMax | fcCurrent > fc.CurrMax | fcCurrent < 0);

unfeas = (battUnfeas | motorUnfeas | fcUnfeas);
```

8.2 Drivetrain model

```
    function [motorTrq,rpm,outboardLimit] = drivetrain_model(speed,acc,...
    boatData,dragCurve,propeller)

%% -- Input --
% speed: Boat speed, m/s
% acc: Boat acceleration, m/s^2
```

```
% boatData: structures containing data
% dragCurve: structures containing drag curve parameters (calmWater,
% lowDrag, middleDrag, highDrag)

%% --Output--
% motorPower: Watt
% outboardLimits: boulean

%% Drag curve of the hull
A = dragCurve.A;
B = dragCurve.B;
C = dragCurve.C;
% A = 50;
% B = 78;
% C = 0.5;
kts_data = linspace(0,20,21); % speed data - drag curve
force_data = A + B.*kts_data + C.*kts_data.^2;% thrust data - drag curve

kts = speed/0.514444; % speed in knots

%% Longitudinal dynamic
dragResistance = interp1(kts_data,force_data,kts,'spline');
propellerThrust = m*acc + dragResistance;

% Foundamental thrust equation
% T = K_T.*(rho.*(RPM./60).^2.*(D).^4);

rpm = (60*propellerThrust^(1/2))/(propeller.d^2*propeller.kT^(1/2)*1000^(1/2));

% Foundamental torque equation
% torque = K_Q.*(rho.*(RPM./60).^2.*(D).^5); %Nm

motorTrq = propeller.kQ .*(1000.*(rpm./60)^2 .*propeller.d^5);
```

8.3 ECMS strategy function

```
    function [battPowerOpt,eqFuelConsumption] = ecmsStrategy(x,u,w,batt,fc,em, ...
    boatData,tank,dragCurve,propeller)

speed = w(1);
acc = w(2);
eqFactor = u;


    [x_next,h2_flowRate,componentsUnfeas,~,fcPower,~,~] = powertrain_model(x, ...
        battPower,[speed acc],batt,fc,em, boatData,tank,dragCurve,propeller);

    % SOC boundary
    unfeas = (x_next(1) < 0.2 | x_next(1) > 0.96);
```

```
    % FC optimal region
    unfeas = (fcPower < 200);

    % Hamiltonian formulation
    SOC = repmat(x(1),1,discretizationFactor);
    SOC_next = x_next(:,1)';
    eqFuelConsumption = h2_flowRate + eqFactor.*(SOC - SOC_next);

    % Unfeasibility
    eqFuelConsumption(unfeas) = 1e-2;
    eqFuelConsumption(componentsUnfeas) = 1;

[~,idx] = min(eqFuelConsumption);

%% Optimal Value %%
battPowerOpt = battPower{1}(idx);
```

Bibliography

[1] Yacht Club de Monaco. Monaco energy boat challenge.

[2] Lino Guzzella and Antonio Sciarretta. *Vehicle Propulsion System.* Springer Heidelberg New York Dordrecht London, 2005.

[3] Y. Huang, S. Xu, X. Wang, M. Wu, and H. Peng. A review of power management strategies and component sizing methods for hybrid vehicles. *Renewable and Sustainable Energy Reviews*, 96:132–144, November 2018.

[4] D. G. Luenberger. *Introduction to Dynamic Systems: Theory, Models, and Applications.* John Wiley Sons, New York, 1979.

[5] MathWorks. Fuel cell electrical system.

[6] MathWorks. Simscape.

[7] Giorgio Romano. Energy management strategy of fuel cell hybrid electric vehicles based on dynamic programming and neural networks. Master's thesis, Politecnico di Torino, 2021.

[8] T. Teng, X. Zhang, H. Dong, and Q. Xue. A comprehensive review of energy management optimization strategies for fuel cell passenger vehicle. *International Journal of Hydrogen Energy*, 45(39):20293–20303, August 2020.

[9] Xiuliang Zhao, Lei Wang, Yinglong Zhou, Bangxiong Pan, Ruochen Wang, Limei Wang, and Xueqing Yan. Energy management strategies for fuel cell hybrid electric vehicles: Classification, comparison, and outlook. *Energy Conversion and Management*, 270:116179, 2022.